PCB PIEZOTRONICS
AN AMPHENOL COMPANY

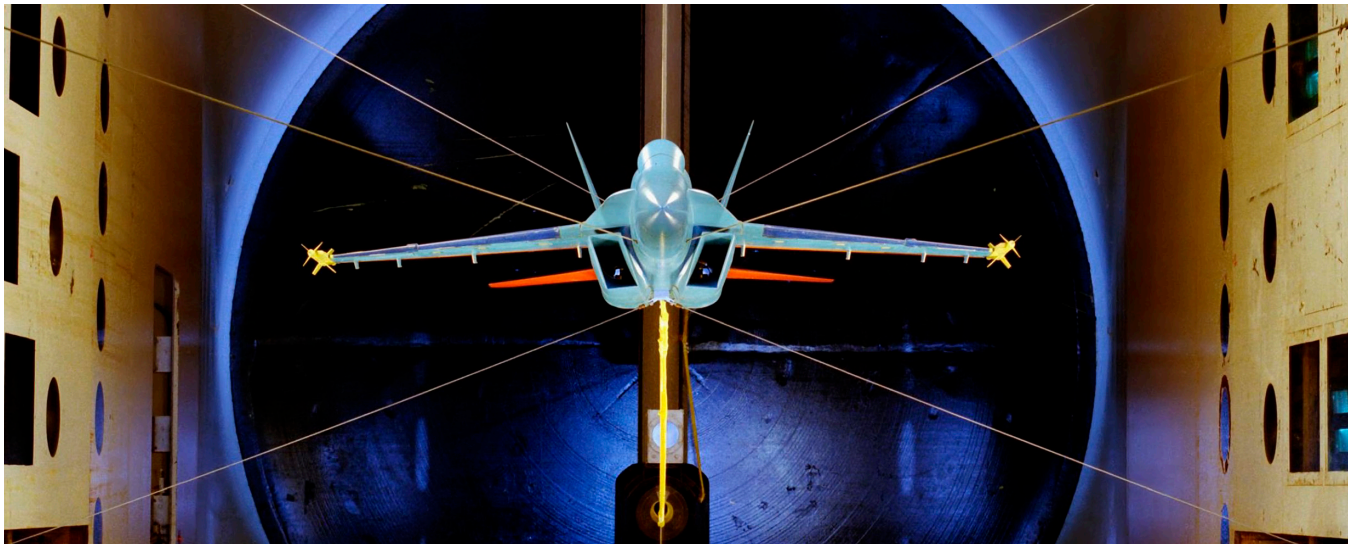

Influence of Mounting on the Accuracy of Piezoelectric Pressure Measurements for Hypersonic Boundary Layer Transition

Written By

David J. Ort
Jeffrey J. Dosch
PCB Piezotronics, Depew, NY, 14043, USA

Influence of Mounting on the Accuracy of Piezoelectric Pressure Measurements for Hypersonic Boundary Layer Transition

David J. Ort,[1] and Jeffrey J. Dosch[2]
PCB Piezotronics, Depew, NY, 14043, USA

The Model 132 pressure sensor, manufactured by PCB Piezotronics, has proven to be a critically important tool in understanding hypersonic boundary layer transition (BLT). The Model 132 was originally developed as a shock wave time-of-arrival trigger sensor, and as such, the factors that influence the accuracy in the BLT environment have not been well explored. Arguably, the most important factor is the mounting method, as this will affect electrical isolation, vibration and strain isolation, effective sensing area, pressure sensitivity, and frequency response. To demonstrate mounting influence on sensor performance, calibration was performed with different mounting materials and techniques. A low pressure shock tube calibration system was used to determine effective area, sensitivity and frequency response with the various mounting methods. Additionally, a sinusoidal acoustic pressure calibrator operating at 250 Hz, corroborates the sensitivity values obtained by the shock tube system.

I. Nomenclature

SUT	=	Sensor Under Test	
BLT	=	Boundary Layer Transition	
T_1, T_2, T_3	=	Normal Stress in 1, 2, and 3 directions	[N/m^2]
d_{33}, d_{31}	=	Piezoelectric charge coefficients	[pC/N]
A	=	Area	[m^2]
Q	=	Electrical Charge	[pC]
FEM	=	Finite Element Model	

II. Introduction

For decades, the measurement of pressure fluctuations associated with second mode Boundary Layer Transition (BLT) has proved an elusive challenge. Available pressure sensors had effective diameters too large for adequate spatial resolution of short acoustic wavelengths, insufficient noise floor to detect small pressure fluctuations, and most importantly had insufficient high frequency response needed to detect acoustic pressures at frequencies of 400 kHz or more. Over the past 10 years, numerous research organizations have had success in detecting second mode pressure fluctuations using a fast-response micro pressure sensor manufactured by PCB Piezotronics [1-9]. The Model 132 micro pressure sensor was developed initially as shock wave time-of-arrival trigger sensor. Three basic requirements for this trigger application are: small sensing area, a fast step response, and relatively consistent sensitivity between sensors. The fast response is ensured through high resonant frequency. Minimal sensing area is needed for fast step response of a shock wave passing across the sensor's diaphragm. Relatively consistent sensitivity is needed to ensure consistent trigger of the shock event. The accuracy of the pressure measurement is of lesser importance.

In spite of the limitations this "trigger sensor", the sensor has been extremely successful in detecting frequencies associated BLT pressure fluctuations and has been a useful tool in understanding fundamental mechanisms of BLT [1-9]. However, there is unacceptable uncertainty in the accuracy of pressure amplitude, leading to uncertainty in correlating experimental data with analytic models.

In general, factors that can influence pressure accuracy include sensor noise floor, effective sensing area, amplitude linearity, electrical and magnetic interference, sensitivity calibration value, flatness of frequency response,

[1] R&D Engineer, Research and Development.
[2] Technical Director, Research and Development.

acceleration sensitivity, and influence of structural strain. Mounting is of particular importance because it has an effect on all these factors.

The present work characterizes the influence of mounting technique using a shock tube calibration system developed at PCB Piezotronics. This paper is organized as follows: sensor design and construction is described; the shock tube for calibrating the microsensor is explained; and the influence of mounting on the 132B38 performance is demonstrated using the shock tube calibration system.

III. Microsensor Design and Construction

A piezoceramic crystal produces an electrical charge in response to applied stress. Piezoceramic material is not inherently piezoelectric. As part of the manufacture process, a high voltage poling operation orients crystal domains to produce useful piezoelectric response. The poling orientation is tailored to produce a crystal that responds to normal stress or to shear stress. The 132 sensor uses a crystal that responds to normal stress – and is insensitive to shear. In this case poling is along the 3-axis, the electrode charge pickup is on a face normal to the 3-axis (Fig. 1). The crystal will produce charge Q in response to normal stress T in proportion to the piezoelectric d coefficient according to the following equation [13]:

$$Q/A = T_1 d_{31} + T_2 d_{31} + T_3 d_{33} \qquad \text{(Eq. 1)}$$

Typical values for d_{33} and d_{31} in piezoceramic are respectively 374 pC/N and -171 pC/N [13]. Note that the sign of the charge coefficient in the radial direction d_{31} is opposite to the axial direction d_{33}.

The 132B38 microsensor is comprised of cylindrical piezoceramic crystal potted in an epoxy matrix, a microelectronic preamplifier integrally bonded to the crystal, and a coaxial signal cable, all enclosed in a tubular stainless steel housing (Fig. 2). Pressure acting on the face of the piezoceramic – indicated by stress T_3 in Fig. 1 – will produce an electrical charge output Q in proportion to pressure. The ICP® voltage amplifier converts the charge to a low-impedance voltage signal. This close integration of microelectronics is the key technology that enables miniaturization of the piezoceramic element. By closely locating the electronics, the element is miniaturized while maintaining high sensitivity and high signal-to-noise needed for measurement of low amplitude pressure fluctuations. If the preamplifier were remote, the cable capacitance would overwhelm the low capacitance of the piezoceramic element, resulting in greatly reduced sensitivity and increased noise.

By miniaturizing the piezoceramic, a high resonant frequency is achieved, enabling fast response. The small diameter of the piezoceramic enables accurate spatial resolution of the pressure field. For valid spatial resolution, the effective sensing area must be small relative to the pressure wavelength [10,11]. The 132B38 element diameter is 0.035" (0.81 mm) and this length is equal to the wavelength in air at a frequency of 422 kHz (at 20°C). For a plane wave at 90° incidence to the sensor face, it is expected that the usable upper frequency would about one fourth this frequency or 100 kHz. However, this is not necessarily the upper frequency limit for BLT applications, as demonstrated by Beresh [12] reporting credible measurements to 400 kHz by applying the Corcos correction [10] to spectral data from a 132A31 sensor.

The extreme miniaturization of the 132B38 comes at the cost of accuracy and sensitivity to environmental influences. This is of little importance for time-of-arrival applications, but of great importance for quantifying BLT pressure fluctuations.

The tubular stainless steel housing is connected to signal ground, and there is the possibility of signal noise caused by electrical ground loops. Insulating coating on the sensor can provide electrical isolation and prevention of ground loops.

Piezoceramic is pyroelectric, generating charge in proportion to changing temperature. For blast applications, in order to attenuate the potential influence of blast heat load on the sensor output signal, the 132B38 has a very short low frequency time constant of 45 µsec. This is results in a high-pass filter with -5% signal attenuation at a frequency of 11 kHz and a -3dB attenuation at 3.5 kHz. Standard piezoelectric sensors use quartz (or similar class 32 crystal) which is not pyroelectric so direct pyroelectric response is not an issue. However, quartz has a low piezoelectric coefficient – about 150 times smaller than piezoceramic – and microsensor made from quartz would have insufficient sensitivity and noise floor.

The sensor's desired charge output is a result of pressure T_3 acting on the face the crystal (Fig. 1). In addition, the crystal will produce charge, in accordance with Eq. 1, in response to extraneous compressive stresses T_1 and T_2 acting perpendicular to this face, thus degrading the accuracy. The piezoelectric coefficient in the radial direction d_{31} is of opposite sign to the axial coefficient d_{33}. That is, for hydrostatic pressure – equal pressure T on all faces of the crystal

– the pressure acting in the radial direction *reduces* the charge output. This response to extraneous stress is not a concern for standard-size piezoelectric sensors, which have metal diaphragms, and the piezoelectric crystal is well isolated from the housing.

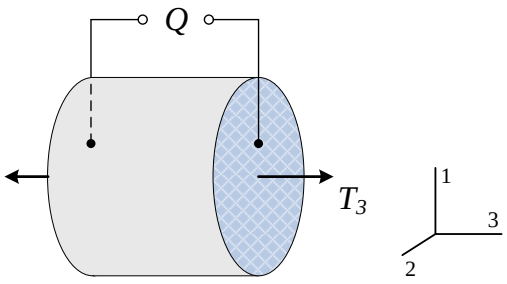

Fig. 1 Piezoceramic charge output.

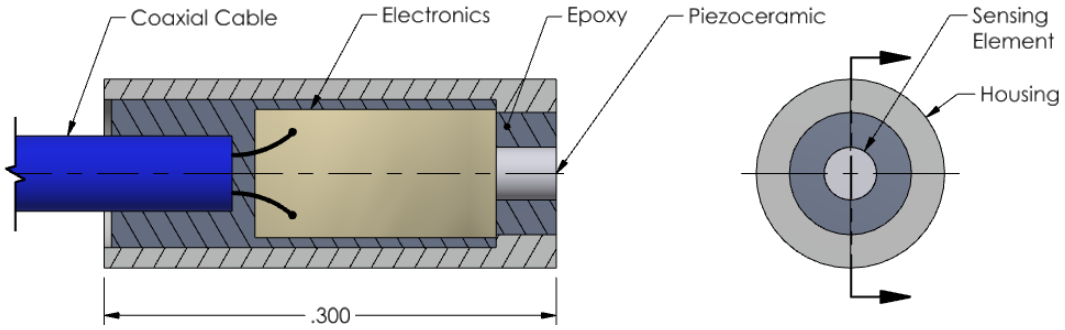

Fig. 2 Model 132B38 construction.

IV. Calibration Systems

Sensitivity and frequency response is obtained from step response in a shock tube. The shock tube system used is a PCB Model 901A10, A.K.A. "Big Blue" (Fig. 3). The shock tube is constructed of a 2" ID pipe with a 12" driver section and 72" driven section. For this work, a 0.001" thick aluminum diaphragm is allowed to naturally burst. This creates a ~4 psi shock step traveling at ~ 1.1 Mach. With these conditions, the step duration is ~0.001 seconds long.

To measure the velocity of the shock wave, two time-of-arrival sensors (PCB model 132A36) are used along the driven section. A PCB Model 134A with a voltage amplifier is used to measure the reflected pressure step. The 134A and amplifier are calibrated as a system with PCB model 903B Dynamic low-pressure calibration system. External sensors measure the atmospheric pressure, humidity, and temperature.

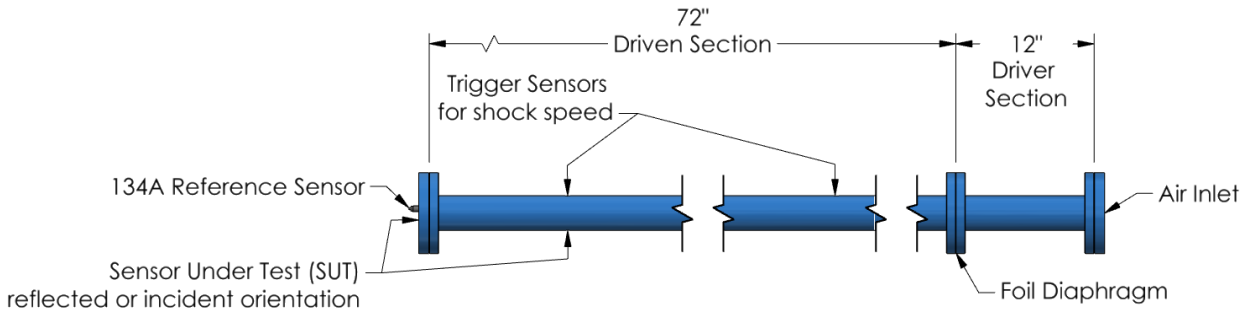

Fig. 3 Shock tube system outline.

The sensor under test (SUT) is mounted in either in an incident position in the sidewall of the shock tube, or in a reflected position at the end of the shock tube (Fig. 4). Calibration in the reflected position has the advantage of near instantaneous pressure, applied uniformly over the entire sensing area. This allows for the calculation of pressure sensitivity and the "true" frequency response. Calibration in the incident position can be used to evaluate the time for a shock wave to pass over the sensing area. The SUT is connected to the input of an ICP® signal conditioner with a "T" on the input connector, so that the signal bypasses the signal conditioner circuitry. The ICP® signal conditioner is set to supply 20mA of constant current. Data is collected at 10 MHz.

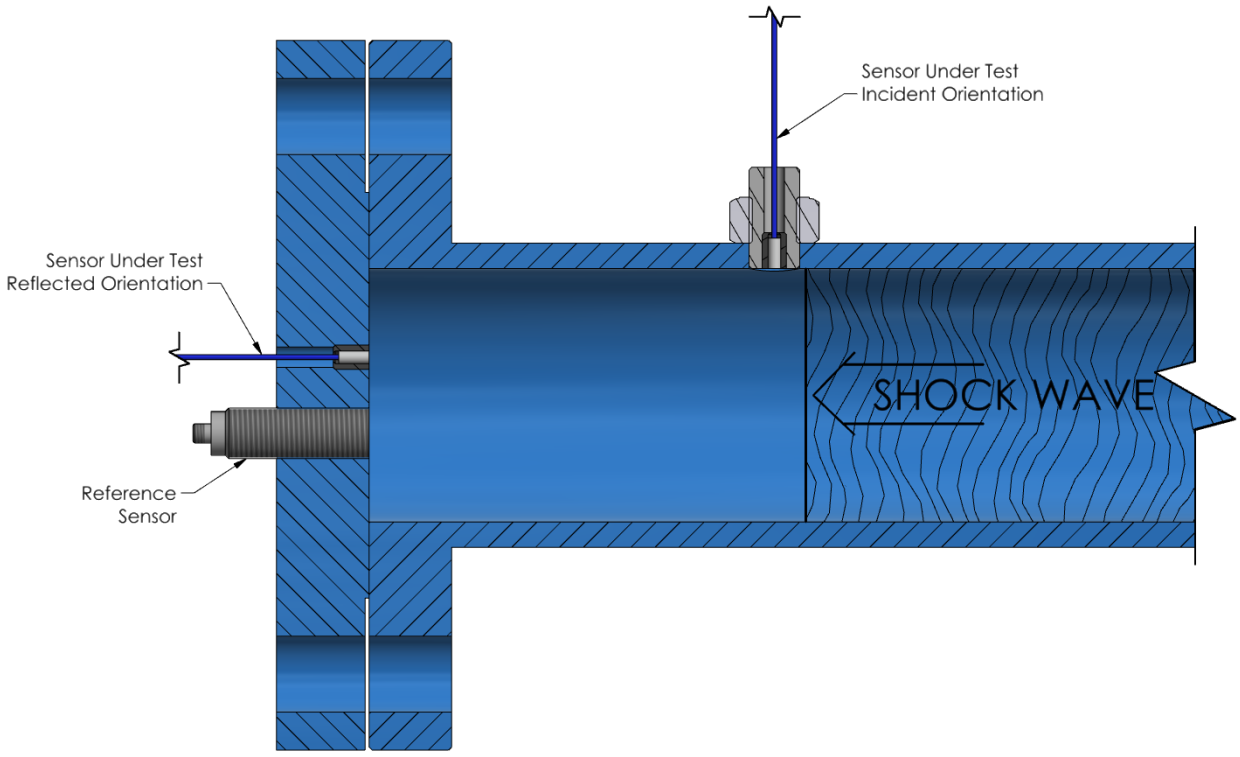

Fig. 4 SUT mounting orientation.

The short time constant of the 132B38 creates a challenge for calculation of pressure sensitivity. Fig. 5a is an example of a step response from a reflected shock wave. The short time constant with associated signal decay, and SUT ringing makes is impossible for a time domain comparison of the SUT Fig. 5a against the reference Fig. 5b. One approach to obtaining a sensitivity value is to convert the time domain data to the frequency domain, scaled to the pressure reference (Fig. 5c). In the frequency domain, a flat region can be averaged and used as a reference pressure sensitivity. In Fig. 5c this is the region marked in red centered at 20kHz.

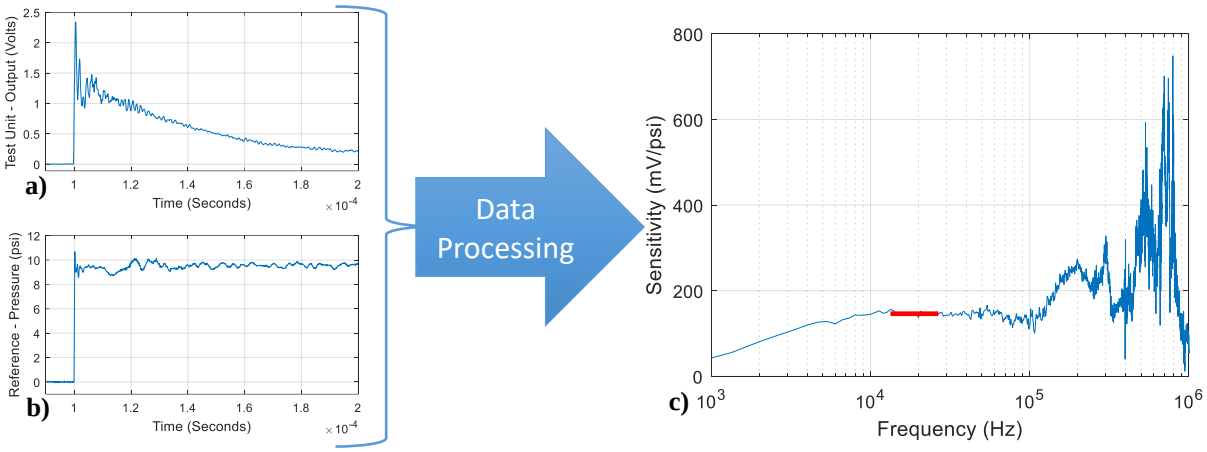

Fig. 5 Data processing a) SUT response b) reference response c) calculated sensitivity vs frequency.

In the present work, a special sensor with extended time constant – designated as X132B38 – was manufactured. The mechanical structure of the X132B38 is exactly the same as the 132B38. The longer time constant equal to 50 msec, allows for the addition of two time domain methods for pressure sensitivity calibration.

First is the time domain sensitivity from the shock tube with SUT mounted in the reflected position. Fig. 6 shows an example of a X132B38 response. After the initial sensor dynamics have settled, the response reaches a flat steady-state step response. This allows a step response value to be obtained for calculation sensitivity. In Fig. 6, the region marked in red, centered at time of 0.55 msec, is averaged for calculation of sensitivity.

The second method uses a standard acoustic calibrator – Larson Davis Model CAL250. The CAL250 generates a harmonic pressure input at a frequency of 250.1 Hz and amplitude of 1.5 mpsi rms (10 Pa rms). Although the pressure amplitude in the CAL250 is low, the sensitivity can be resolved because of the extremely low noise floor of the 132 sensor.

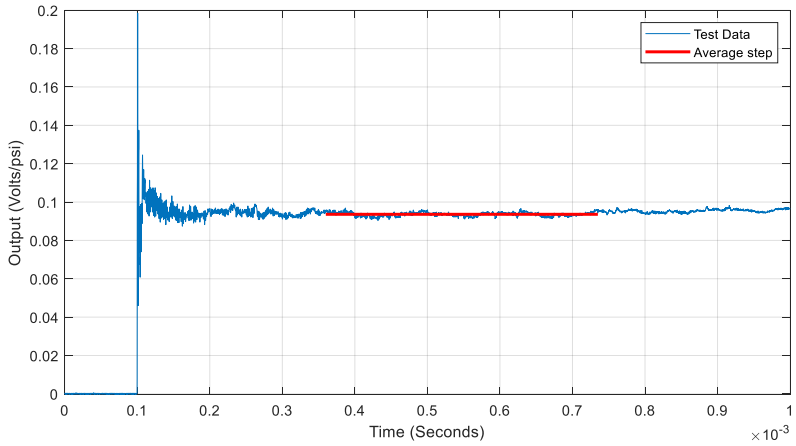

Fig. 6 Time domain data processing.

V. Sensor Performance

The main objective of the study is to characterize how sensor performance is influenced by mounting method. The sensor performances studied are effective sensing area, pressure sensitivity, and frequency response. The two mounting methods are Adhesive (Fig. 7) and Rubber Sleeve (Fig. 8). There are several variations of each of these mounting methods with variation in adhesive type and mounting hole diameter. Below is the mounting procedure for each method.

Adhesive mounting Procedure

- The sensors cable is fed through the mounting hole.
- Adhesive is applied around the outside of the sensor.
- The sensor is placed in the hole and spun around.
- Tape is applied over the diaphragm to position it flush with the structure while curing.

Rubber sleeve mounting procedure

- Rubber tubing is an interference fit into the mounting hole.
- The tubing is pressed into the hole and cut flush with the surface.
- The sensor is an interference fit into the rubber tubing and is pressed in until flush.

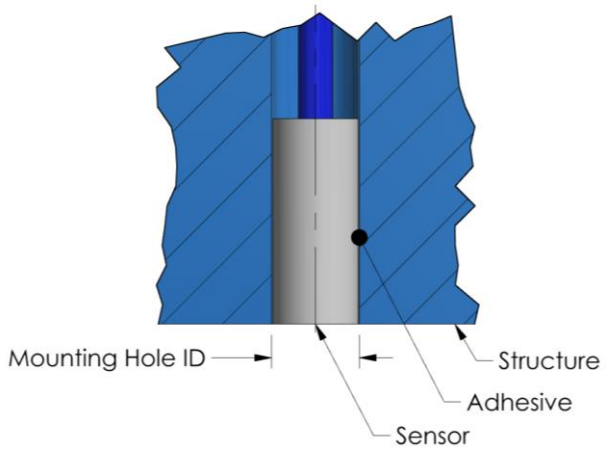

Fig. 7 Adhesive mounting.

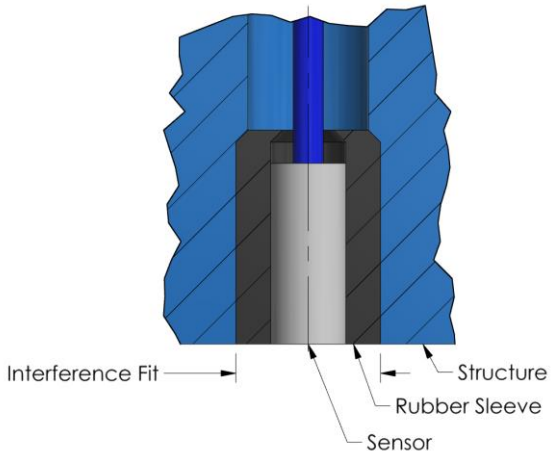

Fig. 8 Rubber sleeve mounting.

A. Effective Sensing Area

Effective sensing area was determined from measurements with the SUT mounted in the incident shock tube position (Fig. 4). Conceptually, the larger the sensing area, the longer it takes for the shock wave to pass over the sensing area, resulting in a longer time for the sensor to achieve step response. This approach is valid because the sensor's step response – <0.7 µsec measured in the reflected position – is significantly faster than the time for wave passage across the piezoceramic sensing element.

Ideally, the sensing area is equal to the 0.035" (0.89 mm) diameter of the piezoceramic crystal. However, acoustic pressure may transfer radial stress from the area surrounding the crystal to make the effective sensing area larger than the physical sensing element (Fig. 9).

In this study, we measured the effective area for two mounting cases. In the first case, the sensor was adhesively mounted in a 0.1285" (3.264 mm) hole as recommended per the 132B38 Product Manual. In the second case, the sensor was mounted in a rubber isolator, an approach similar to that used by BLT researchers to isolate the sensor from structural vibration.

To determine the effective sensing area, a regression is used to fit the measured incident response to a theoretical model function (Fig. 10). The model function is the net pressure force acting on circular area due a shock wave passing over the sensing area travelling at a known speed (Fig. 9). This approach to determining effective area is similar to work done by Dennis C. Berridge at Purdue University, used in measuring the effective area of a PCB Model 132A31 microsensor [3].

For the "factory recommended" RTV mounting case, an effective sensing diameter is 0.0382" (0.97 mm) was determined. This is approximately 10% larger than the crystal diameter.

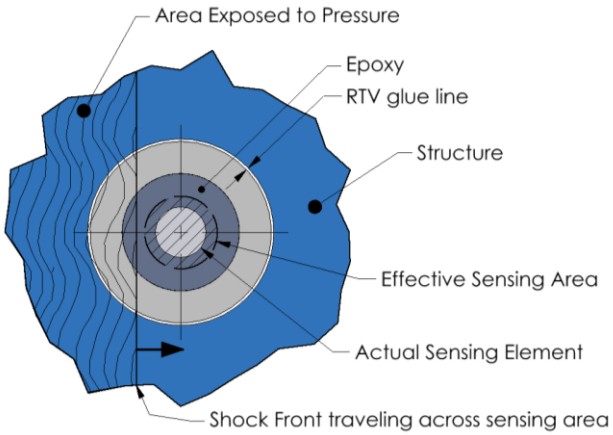

Fig. 9 RTV mount, test overview.

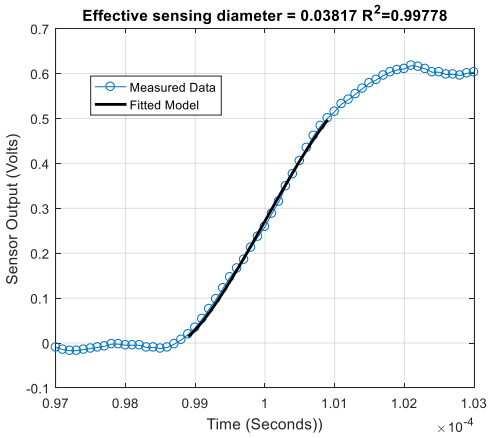

Fig. 10 Test data vs sensor model.

In the next case, we determined the effective sensing area when the sensor is mounted in a rubber sleeve (Fig. 11). For this test, the X132B38 with extended time constant of 50 msec was used (time constant for a standard 132B38 is 45 µsec). The longer time constant permits observation of the step response to 1 msec without significant signal decay. One observation is a dip in the incident response preceding the rise (Fig. 12a). To better understand this anomalous response, a piezoelectric-structural FEM was developed to solve for the sensor output. The FEM is a series of static analyses with a progressing area of applied pressure. Underlying assumption in this analysis is that sensor dynamics has a minimal effect on incident response.

There is good correlation between the FEM and test data (Fig. 12a). They both show a negative dip before the step and an overshoot after the step. The anomalous dip in the response can be understood as follows. When the shock wave is passing over the face of the assembly, pressure is first applied to an area of the rubber causing a negative dip (Fig. 12b). Next, when the shock wave has passed over the sensing element, the signal reaches its peak value (Fig. 12c). Last, when the shock is passing over the remainder of the rubber, the signal reaches its slightly reduced final value (Fig. 12d).

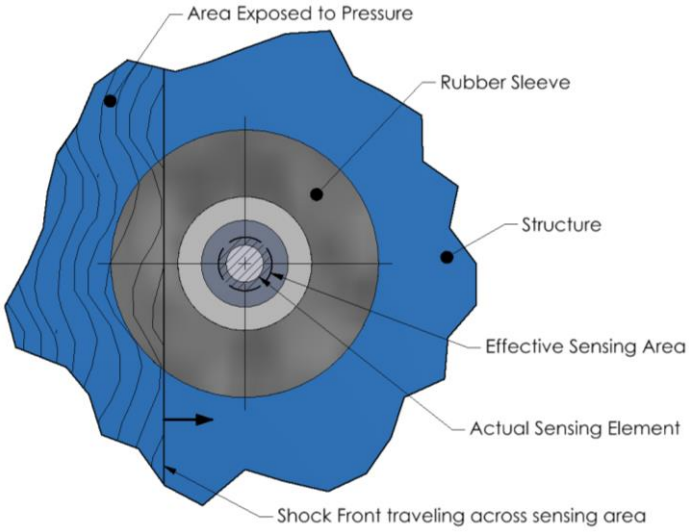

Fig. 11 Rubber sleeve mount, test overview.

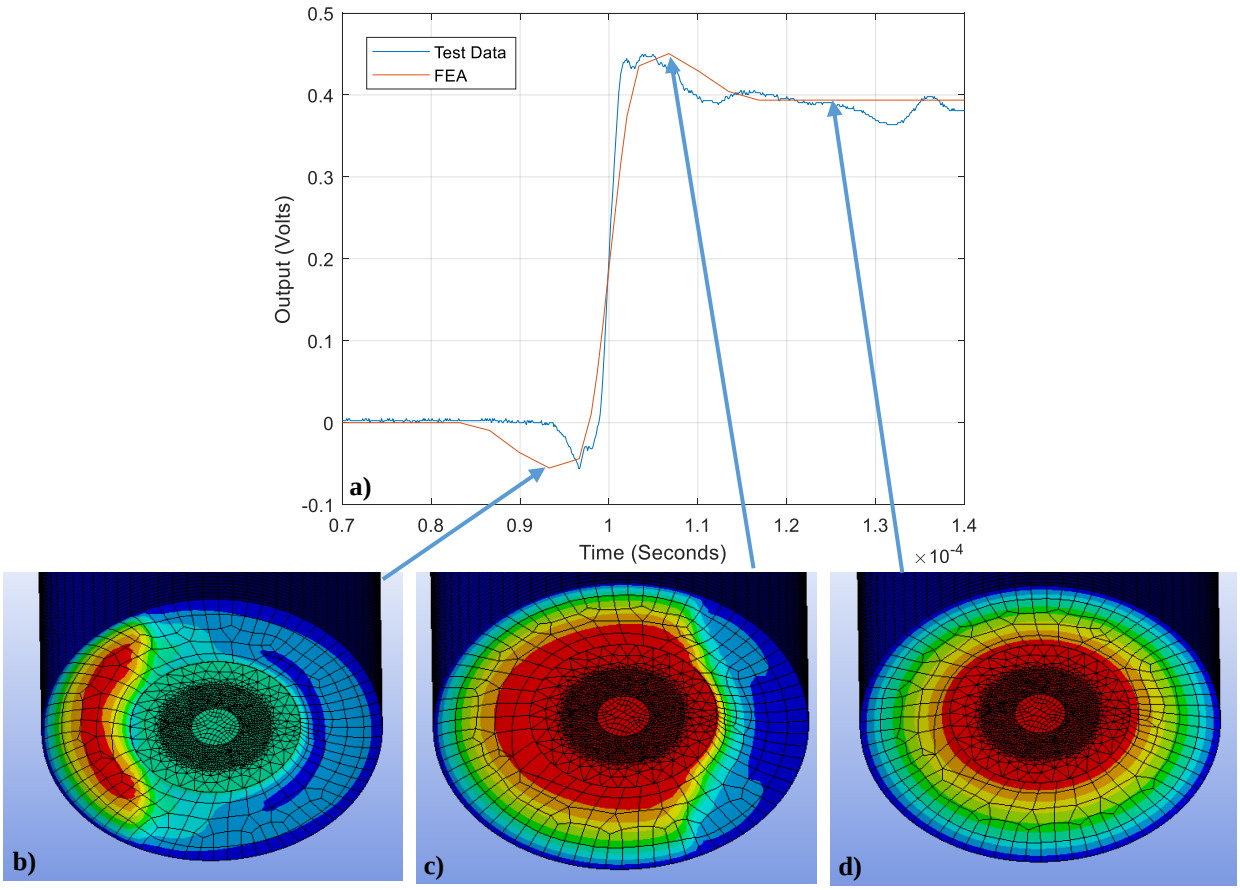

Fig. 12 FEM vs Test data a) sensor response b) deformation at dip c) deformation at peak d) deformation at steady state.

The dip and over shoot in the signal is caused by the piezoceramic's sensitivity to stress in the radial direction. According to Eq. 1, compressive radial stress will reduce charge output, resulting in a dip in response. When pressure is applied to the rubber isolator, the Poisson effect in the rubber causes compressive stress on the outside diameter of the piezoceramic element (Fig. 13). The conclusion is that, depending on the mechanical properties of the rubber isolator, the effective area may become ill defined and the sensor may respond to pressure acting outside the crystal area. The pressure-stress influence of the mount makes determination of sensing area complicated because depending on where the pressure is acting, pressure may have a positive or negative influence on signal output (albeit the dip in the negative direction is considerably smaller than positive). Another complication is the frequency response, due to pressure acting on the rubber sensing area, most likely has a response different from the inner area.

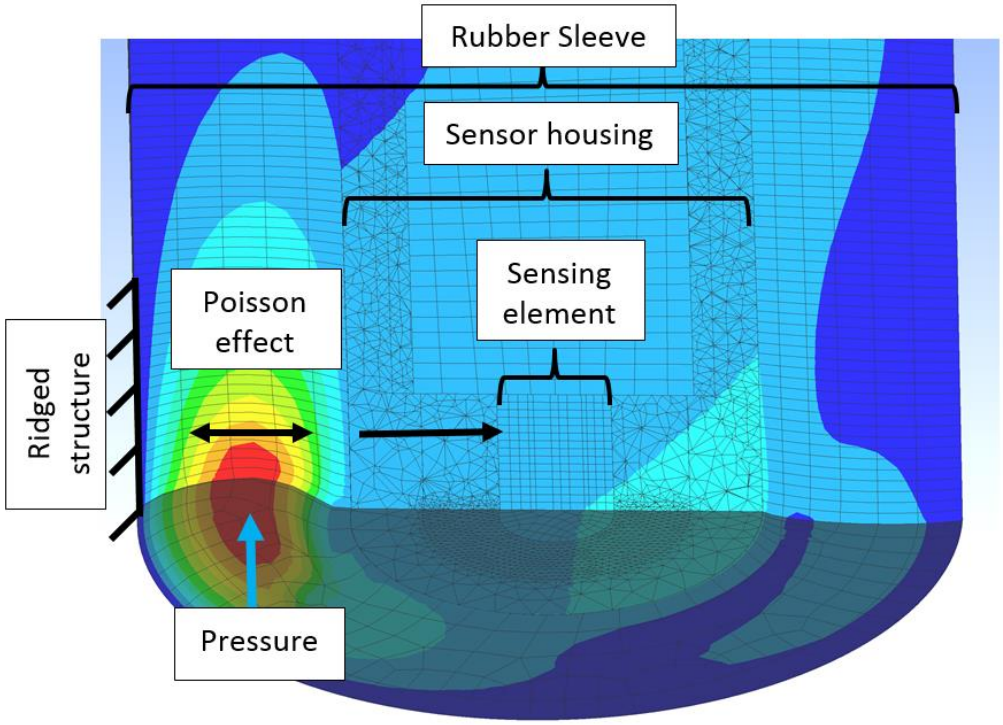

Fig. 13 Cross Section of FEM during response dip.

B. Pressure Sensitivity

All three of the calibration methods described in Section IV were used to evaluate the pressure sensitivity of the X132B38 microsensor. The three calibration methods were: 1) time domain step response in reflected position; 2) frequency domain response, centered at 20kHz, and measured in the reflected position; and 3) pressure sensitivity at 250 Hz measured in an acoustic calibrator (CAL250). A total of five mounting configurations were used (Table 1).

Table 1 Mounting configurations.

Mounting Method	Mounting Material	Material Durometer	Hole size
Rubber Sleeve	Neoprene Rubber	80A	n/a
Rubber Sleeve	Neoprene Rubber	60A	n/a
Rubber Sleeve	Buna-N Rubber	60A	n/a
Adhesive	RTV 118	n/a	.1285”
Adhesive	Nail Polish Wet and Wild, Clear	n/a	.1265”

Sensitivities obtained from the three measurement methods are compared in Fig. 14. These results are from a single sensor and are representative of all three sensors tested. Time domain (orange bars) and CAL250 (blue bars) calibration methods produced the most consistent results with the two methods differing less than 1.75% for all mounting configurations. Consistency with the CAL250 helps to validates the accuracy of the time domain shock tube method through independent test method. CAL250 calibration was not performed on the nail polish mount testing because the sensor could not be removed from the shock tube fixture without destroying it.

There was less agreement of the frequency domain (gray bars) with the CAL250 and time domain shock sensitivities. This can be explained by the use of 20 kHz as the reference point of comparison in the frequency domain method. The 20 kHz frequency was chosen as a reference point because it was assumed that this is flat with frequency. Lack of agreement indicates sensitivity is not constant between 250Hz and 20kHz. This could have been caused by a mechanical resonance of the mounting material. Another cause could be a rate dependent material property of the

mounting material. The nail polish mount produced consistent sensitivities for both the frequency and time domain methods. This mount is the stiffest and has a minimal area exposed to pressure.

Pressure sensitivity obtained with Neoprene 60A and Buna-N 60A mounts are nearly identical when tested by time domain and by CAL250. However, the pressure sensitivity from these two materials obtained by the frequency domain method differ greatly. Both mounting materials have the same durometer. This shows the complex nature of these mounting materials.

In this study, the reflected shock wave calibration of sensitivity was determined at a peak pressure of ~8 psi (55 kPa). Sensitivity determined from the CAL250 was performed at a pressure ~.0015 psi rms (10 Pa rms). The agreement of pressure sensitivity over this large range of pressure suggests the sensor is linear through the range of pressures calibrated and that may be encountered in measurements of BLT phenomenon.

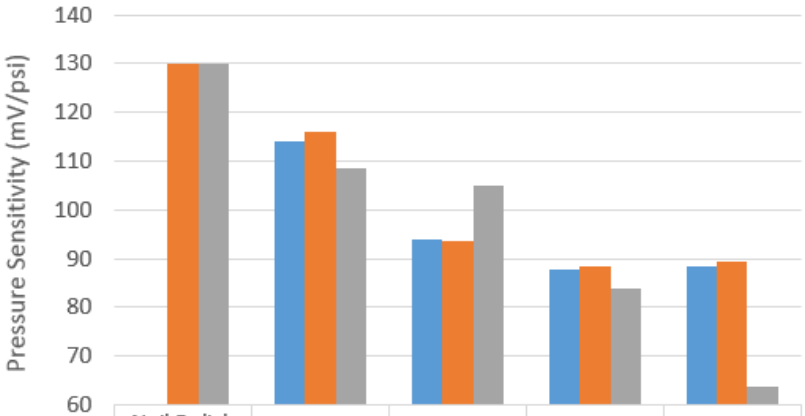

	Nail Polish - Wet and wild, clear	RTV 118 0.1285" ID	Neoprene 80A	Neoprene 60A	Buna-N 60A
Cal 250		114	94	88	88
Time domain	130	116	94	89	89
Frequency domain	130	109	105	84	64

Fig. 14 Pressure sensitivity vs mounting method.

C. Frequency Response

The influence of mounting on frequency response was examined by a single Model 132B38 sensor (SN 25030) using a number of different mounting methods. The sensor was mounted in the reflected orientation and tested with the method discussed in Section IV. These plots are in dB, referenced to the average sensitivity centered at 20 kHz (response sensitivity averaged between 13.3 and 26.7 kHz).

First, we looked at mounting the sensor in a rubber sleeve Fig. 15. Three different materials were tested of varying composition and durometer. It appears that below ~60 kHz, all of the responses are the same independent of the isolator type. All of the responses show an attenuation in response between 20 kHz and 50 kHz. The softest material has an additional peak at ~100 kHz. All three materials have a peak around 300 kHz and multiple peaks above 400 kHz.

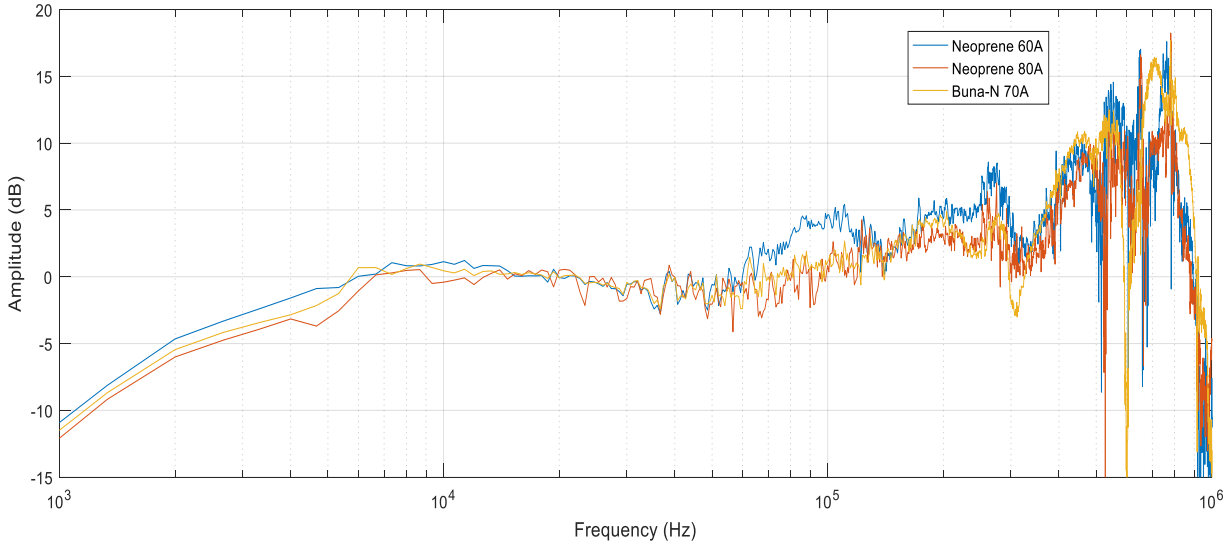

Fig. 15 132B38 frequency response, mounted in rubber.

Next, we looked at adhesive mount of the sensor using RTV 118 (MG Chemicals). Three different diameter holes were used varying from 0.126" to 0.135" (3.20 mm to 3.43 mm). All of the responses are the same below ~20 kHz (Fig. 16). The largest hole has some highly damped dynamics between 20 and 80 kHz. Starting around 80 kHz the middle-sized hole has some amplification in the response. Just above 100 kHz the smallest hole has some sharp peaks valleys in the response. Again all responses have a peak around 300 kHz and there are multiple peaks above 400 kHz. The peaks above 400 kHz appear to be sharper and more consistent than the rubber sleeve mounting.

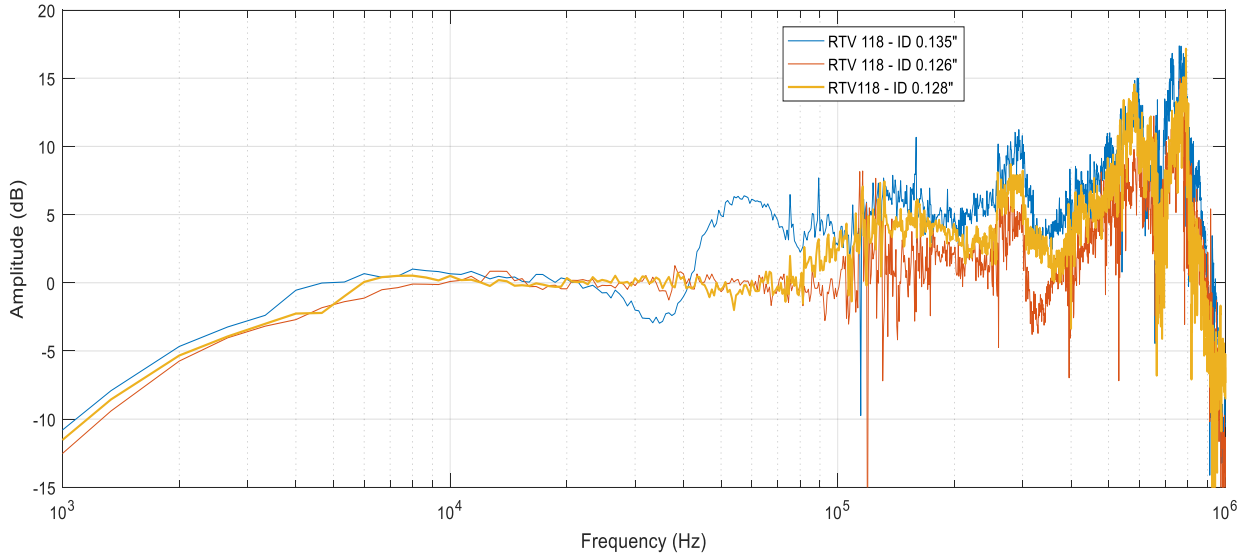

Fig. 16 132B38 frequency response, mounted with RTV.

Last, we mounted the sensor in a hole with Nail polish. The response is flat up to ~100 kHz. Just above 100 kHz there are a few low damping peaks. Similar to all other mounting methods there is a ~300 kHz peak and there are multiple peaks above 400 kHz. With this mounting method, the peaks above 400 kHz are clear and looks like a single large resonant peak with an anti-resonance in the middle. This is a typical response from a multiple coupled mass system.

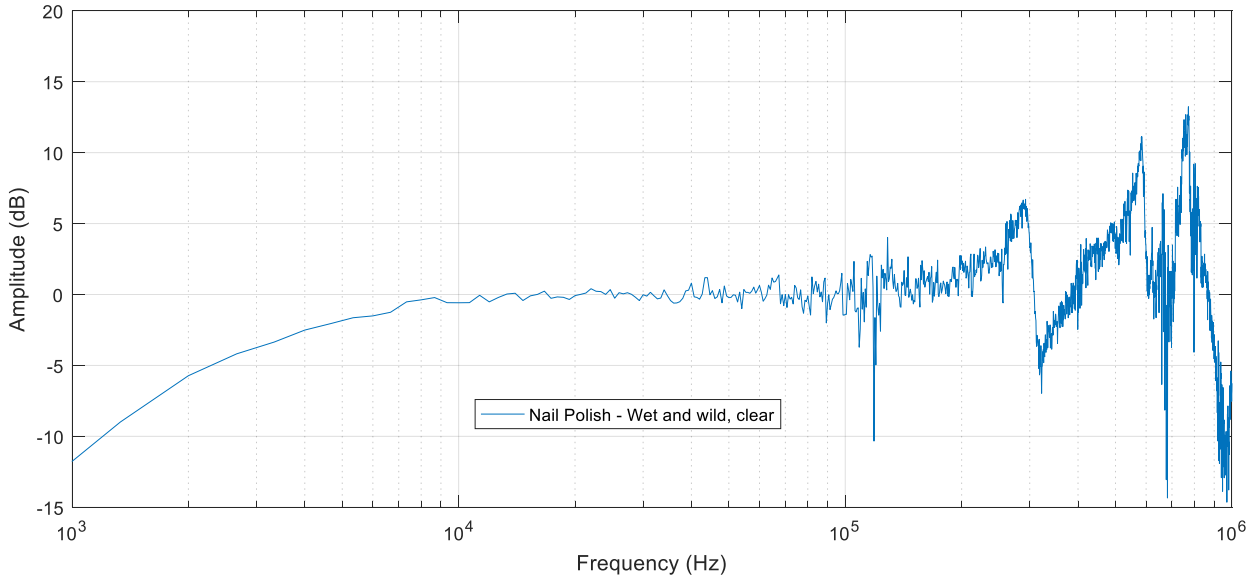

Fig. 17 132B38 frequency response, mounted with nail polish.

VI. Conclusion

Several standard 132B38 and modified X132B38 sensors were calibrated implementing the range of mounting techniques used by researchers in the study of hypersonic boundary layer transition (BLT).

Pressure sensitivity was obtained by three different methods: 1) time domain in a shock tube; 2) frequency domain in a shock tube; and 3) low frequency acoustic calibrator. Calibration at low frequency was made possible by the modified long time constant of the X132B38. Effective area was determined by mounting in the incident position in a shock tube. Frequency response was determined by response of the sensor mounted at the reflected end of a shock tube.

It is concluded that the mount has significant influence on sensitivity and frequency response, and to a lesser extent will influence the effective sensing area. The 300 kHz resonance is part of the sensors dynamics and mounting does not eliminate it.

References

[1] Berridge, D., Ward, C., Wheaton, B., Luersen, R., Chou, A., Abney, A., & Schneider, S. (2012, June). Boundary-layer instability measurements in a Mach-6 quiet tunnel. In *42nd AIAA Fluid Dynamics Conference and Exhibit* (p. 3147).

[2] Beresh, S. J., Henfling, J. F., Spillers, R. W., & Pruett, B. O. (2011). Fluctuating wall pressures measured beneath a supersonic turbulent boundary layer. *Physics of Fluids*, *23*(7), 075110.

[3] Berridge, D. C. (2015). Generating low-pressure shock waves for calibrating high-frequency pressure sensors. Ph.D. Dissertation, Purdue University, West Lafayette Indiana.

[4] Casper, K., Beresh, S., Henfling, J., Spillers, R., Pruett, B., & Schneider, S. (2009, June). Hypersonic wind-tunnel measurements of boundary-layer pressure fluctuations. In *39th AIAA Fluid Dynamics Conference* (p. 4054).

[5] Estorf, M., Radespiel, R., Schneider, S., Johnson, H., & Hein, S. (2008). Surface-pressure measurements of second-mode instability in quiet hypersonic flow. In *46th AIAA Aerospace Sciences Meeting and Exhibit* (p. 1153).

[6] Hedlund, B. E., Houpt, A. W., Gordeyev, S., & Leonov, S. B. (2017). Corner Separation Zone Response to Plasma Actuation in the Hypersonic Boundary Layer over a Compression Ramp. In *48th AIAA Plasmadynamics and Lasers Conference* (p. 3341).

[7] Tanno, H., Komuro, T., Sato, K., Itoh, K., Takahashi, M., & Fujii, K. (2009). Measurement of hypersonic boundary layer transition on cone models in the free-piston shock tunnel HIEST. In *47th AIAA Aerospace Sciences Meeting Including the New Horizons Forum and Aerospace Exposition* (p. 781).

[8] Ward, C., Wheaton, B., Chou, A., Berridge, D., Letterman, L., Luersen, R., & Schneider, S. (2012). Hypersonic boundary-layer transition experiments in the Boeing/AFOSR Mach-6 quiet tunnel. In *50th AIAA aerospace sciences meeting including the new horizons forum and aerospace exposition* (p. 282).

[9] Zhu, Y., Chen, X., Wu, J., Chen, S., Lee, C., & Mohamed, G. E. H. (2017). Aerodynamic Heating in Hypersonic Boundary Layer: Role of Dilatational Waves. In *21st AIAA International Space Planes and Hypersonics Technologies Conference* (p. 2127).

[10] Corcos, G. M. (1963). Resolution of pressure in turbulence. *The Journal of the Acoustical Society of America*, *35*(2), 192-199.
[11] Lueptow, R. M. (1995). Transducer resolution and the turbulent wall pressure spectrum. *The Journal of the Acoustical Society of America*, *97*(1), 370-378.
[12] Beresh, S. J., Henfling, J. F., Spillers, R. W., & Pruett, B. O. (2011). Fluctuating wall pressures measured beneath a supersonic turbulent boundary layer. *Physics of Fluids*, *23*(7), 075110.
[13] Wilson, O. B. (1985). An introduction to the theory and design of sonar transducers. Washington, DC: Naval Sea Systems Command.

PCB PIEZOTRONICS
AN AMPHENOL COMPANY

3425 Walden Avenue, Depew, NY 14043 USA

pcb.com | info@pcb.com | 800 828 8840 | +1 716 684 0001

WPL_69_1121